Evaluation of Orbiter Performance and Nose Heating at Mach 3.8

February 26, 2020

1 Introduction

1.1 3-D orbiter shape

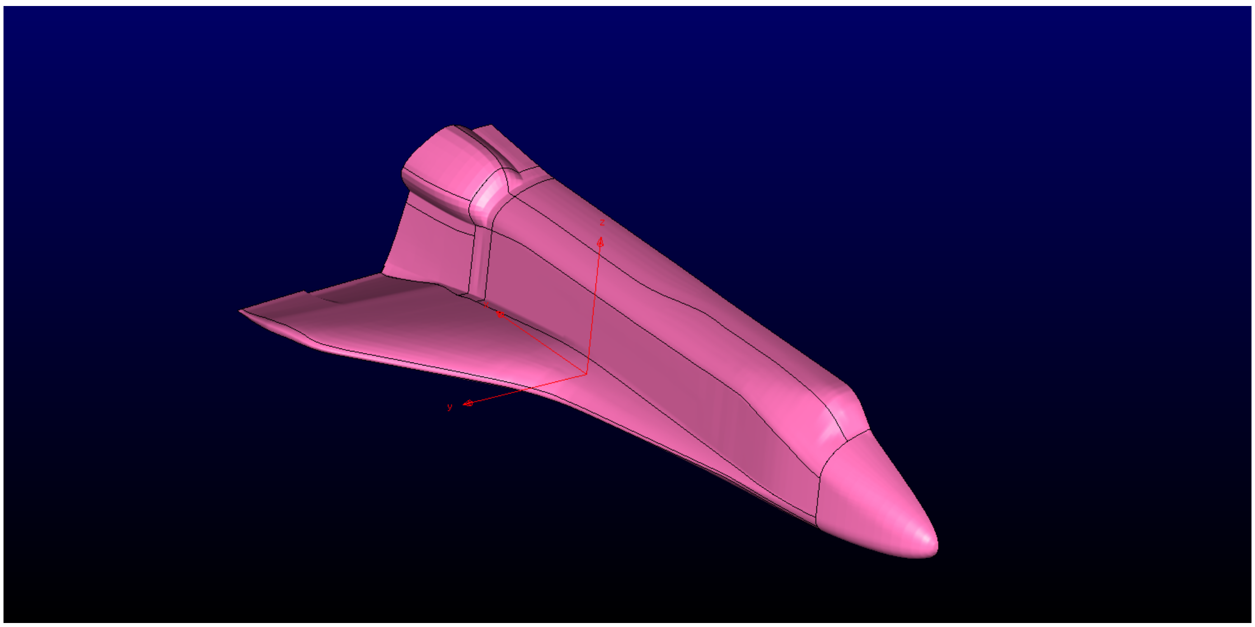

Figure 1: 3-D orbiter

1.2 Data from Published Texts

The equations used to plot the data in figure 2 were from [2]

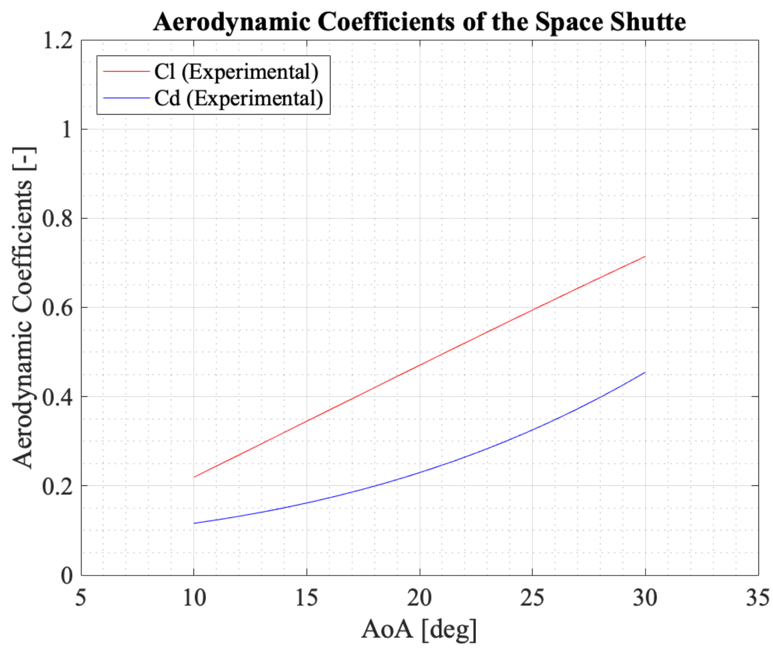

Figure 2: Experimental models and predictions of C_L & C_D for M = 3.8

Table 1: Freestream conditions and expected stagnation conditions at wing/nose LE

Mach number	3.8
Post-shock mach number	0.4407
Pressure p [1]	1090.16 Pa
Temperature T	227.13 K
Density ρ	$0.0167 \text{ kg} \cdot \text{m}^{-3}$
$^{p_2}/_{p_1}$ at M=3.8	16.68
$^{T_2}/_{T_1}$ at M=3.8	3.743
Isentropic $^{p_o}/_{p}$ at M=0.44	1.142
Isentropic $^{T_o}/_{T}$ at M=0.44	1.035
Stagnation pressure	20765.98 Pa $(p \cdot {}^{p_2}/_{p_1} \cdot {}^{p_o}/_{p})$
Stagnation temperature	883.303 K $(T \cdot {}^{T_2}/_{T_1} \cdot {}^{T_o}/_{T})$

p, T, ρ: at 100,000 ft from 1976 Digital Dutch Standard Atmospheric Calculator (URL: https://www.digitaldutch.com/atmoscalc/)

Isentropic relations and pressure/temp discontinuity across shock: From appendix A of Modern Compressible Flow by J.D. Anderson [1].

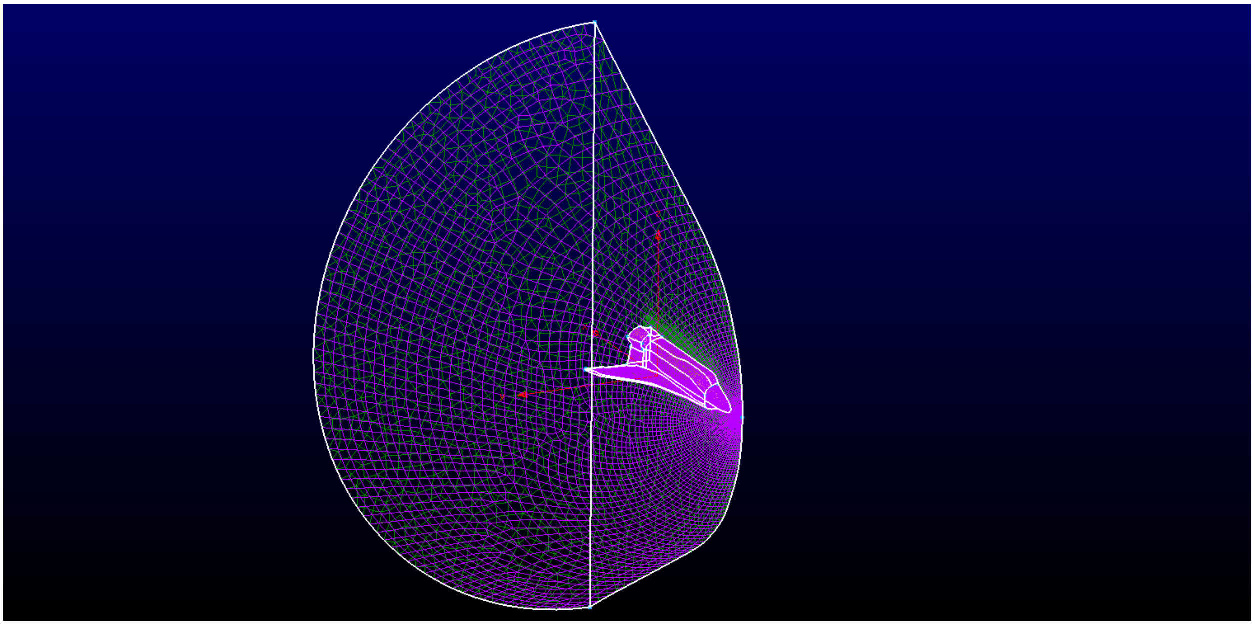

Figure 3: Entire grid of the orbiter

2 Methodology

2.1 Shots of the Orbiter grid

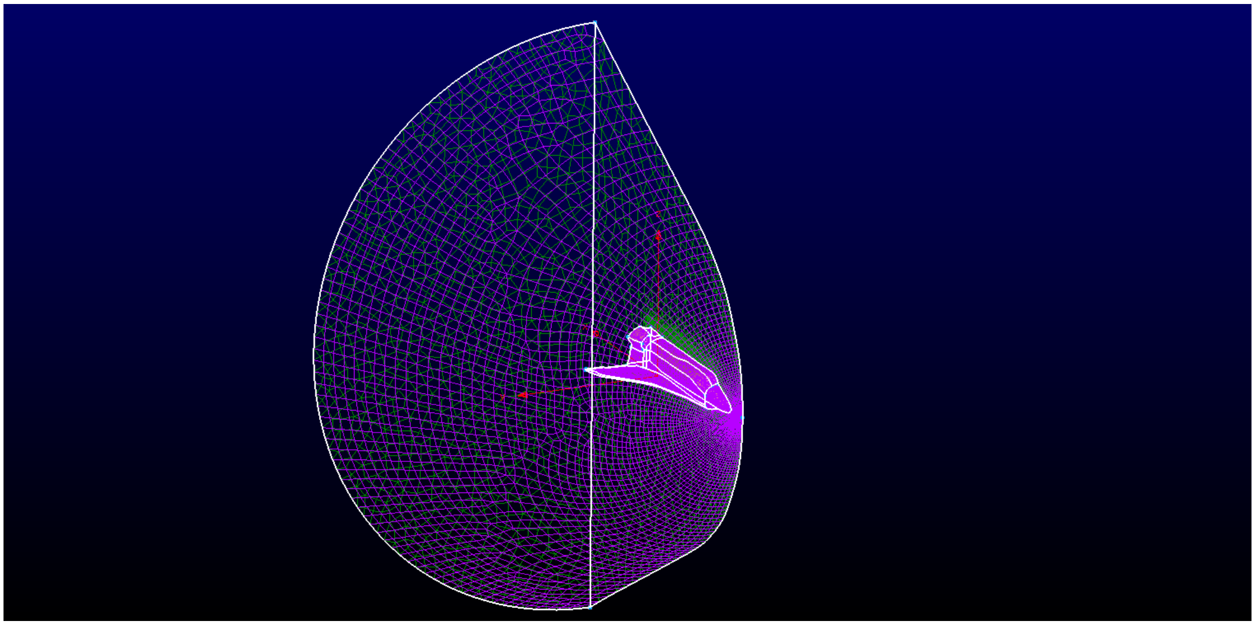

Figure 4: Entire grid of the orbiter

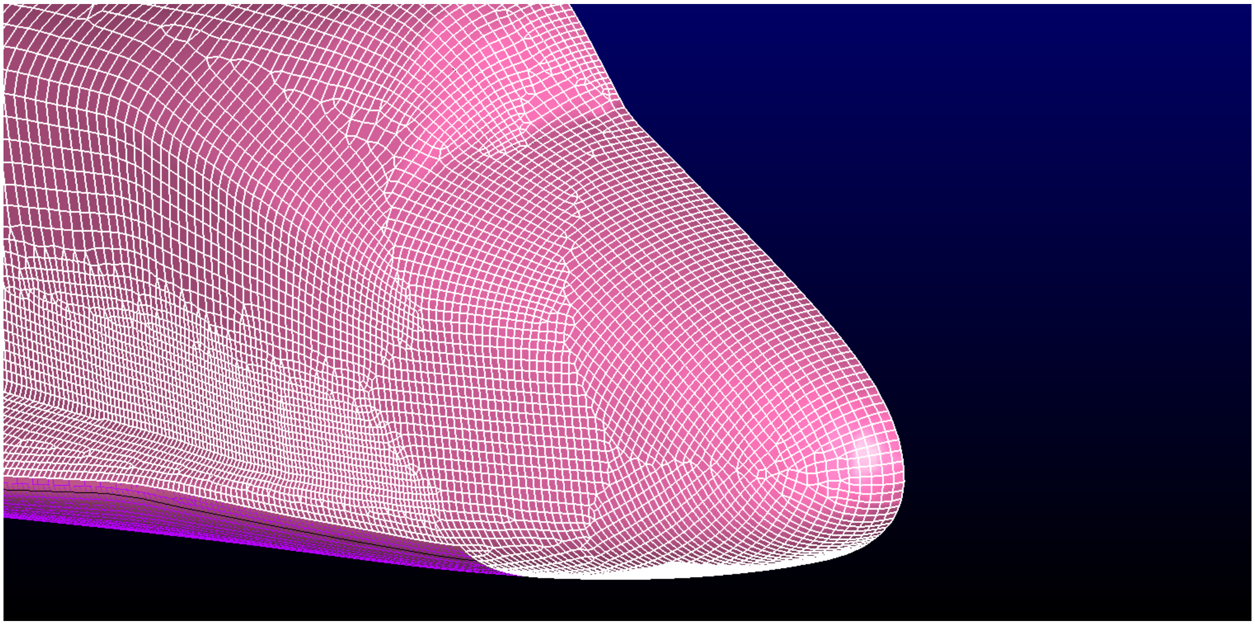

Figure 5: Nose of the orbiter

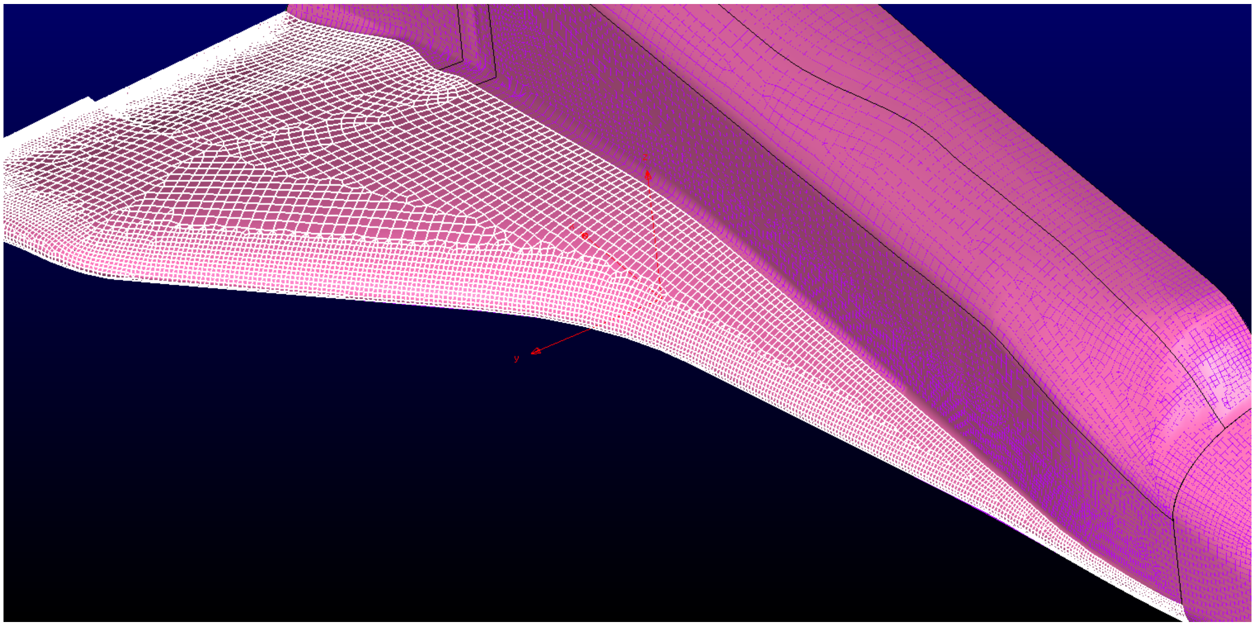

Figure 6: Midspan of the wing of the orbiter

2.2 Fluent setup

Table 2: General grid information

Cell count	1,375,480 Cells
Min/max included angles	**max**: 179.844 deg **min**: 0.06222 deg
Normal-to-wall spacing	$\boldsymbol{\Delta}\mathbf{s} = 0.001$
Boundary conditions	**Inlet/hemispherical shell**: pressure far-field **Outlet/back of hemispherical shell**: pressure outlet **Orbiter surface (including backside)**: wall **Plane of Symmetry**: symmetry
Reference values	**Area**: 257.47 [m^2] **Density**: 1.672e-2 [kgm^{-3}] **Enthalpy**: 8.907e+5 [Jkg^{-3}] **Length**: 38.424 [m] **Gauage pressure**: 0 [Pa] **Temperature**: 227.13 [K] **Velocity**: 1147.86 [m/s] **Viscosity**: 1.789e-05 [$kgm^{-1}s^{-1}$] **Ratio of specific heat**: 1.4
Submodels	**Numerical Scheme**: Implicit AUSM
Method and Accuracy	**Gradient**: least-squares cell based **Flow**: first order upwind

3 Results

3.1 Proof of convergence history

Pleas see Appendix

3.2 Table of final lift and drag coefficients and related forces

Case	C_L [-]	C_D [-]
10	0.143	0.075
20	0.341	0.174
30	0.545	0.371
Adapted 20	0.342	0.173

3.3 Plot of lift and drag and L/D vs. AOA with peak L/D identified

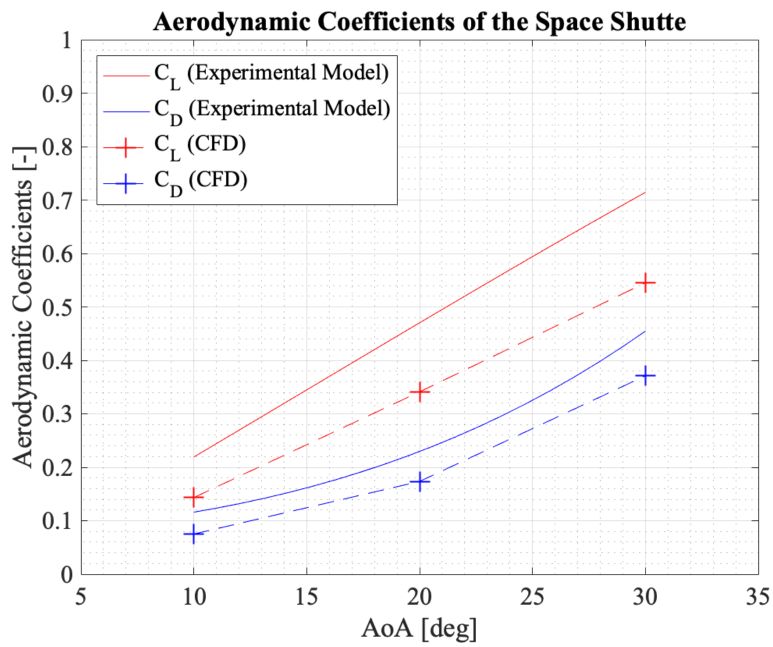

Figure 7: Comparison of the C_L and C_D results from the experimental model and the CFD cases ran

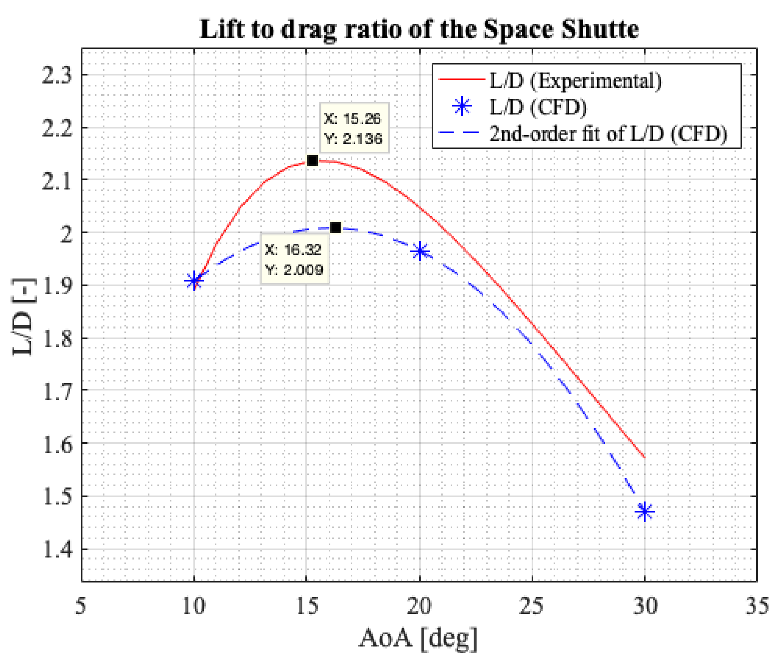

Figure 8: Comparison of the lift-to-drag ratios from the experimental model and the CFD cases ran

3.4 Pressure and temperature contours with streamlines

3.4.1 AoA = 10°

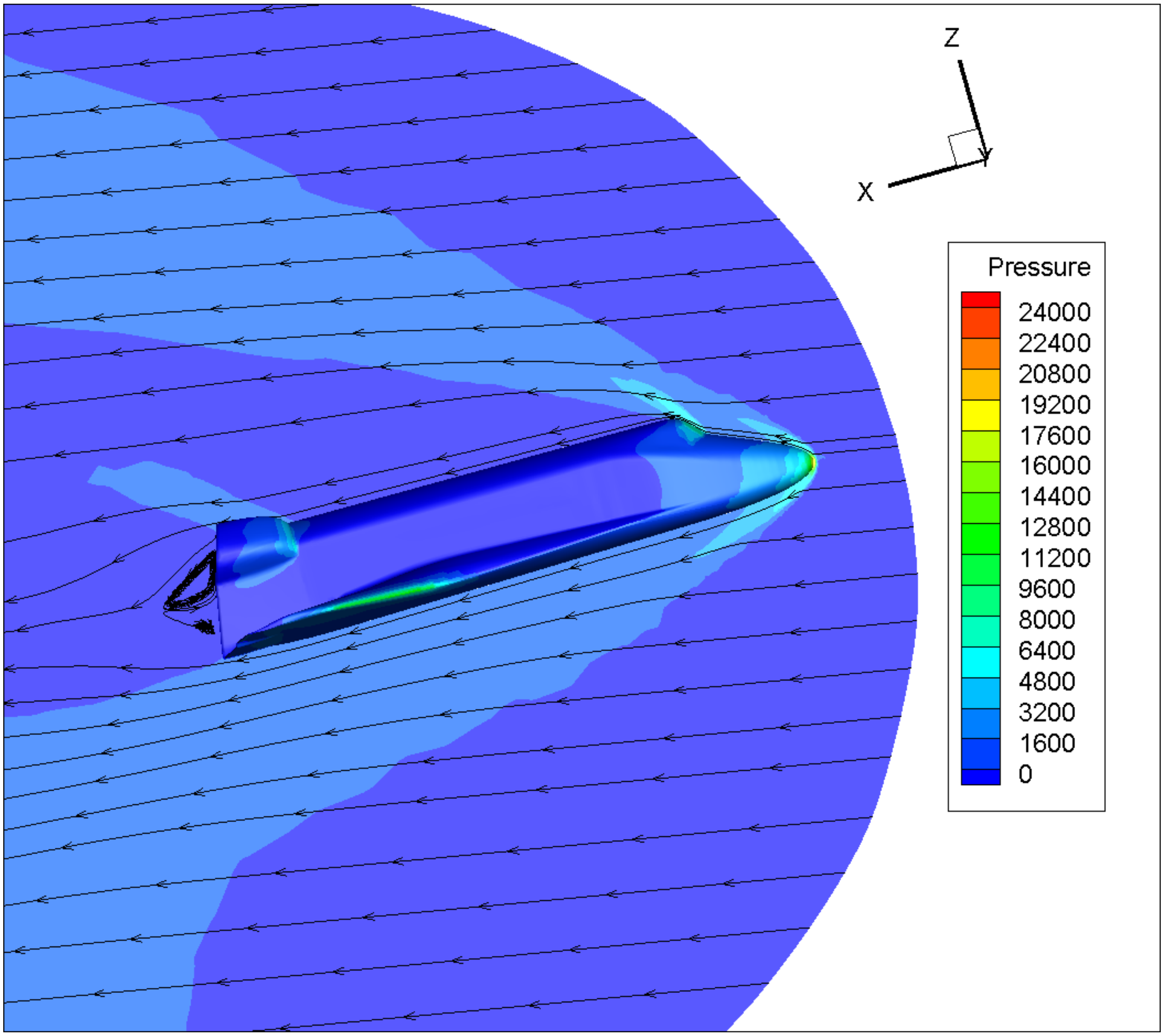

Figure 9: Pressure contour at the symmetry plane of the orbiter at 10 degs AoA

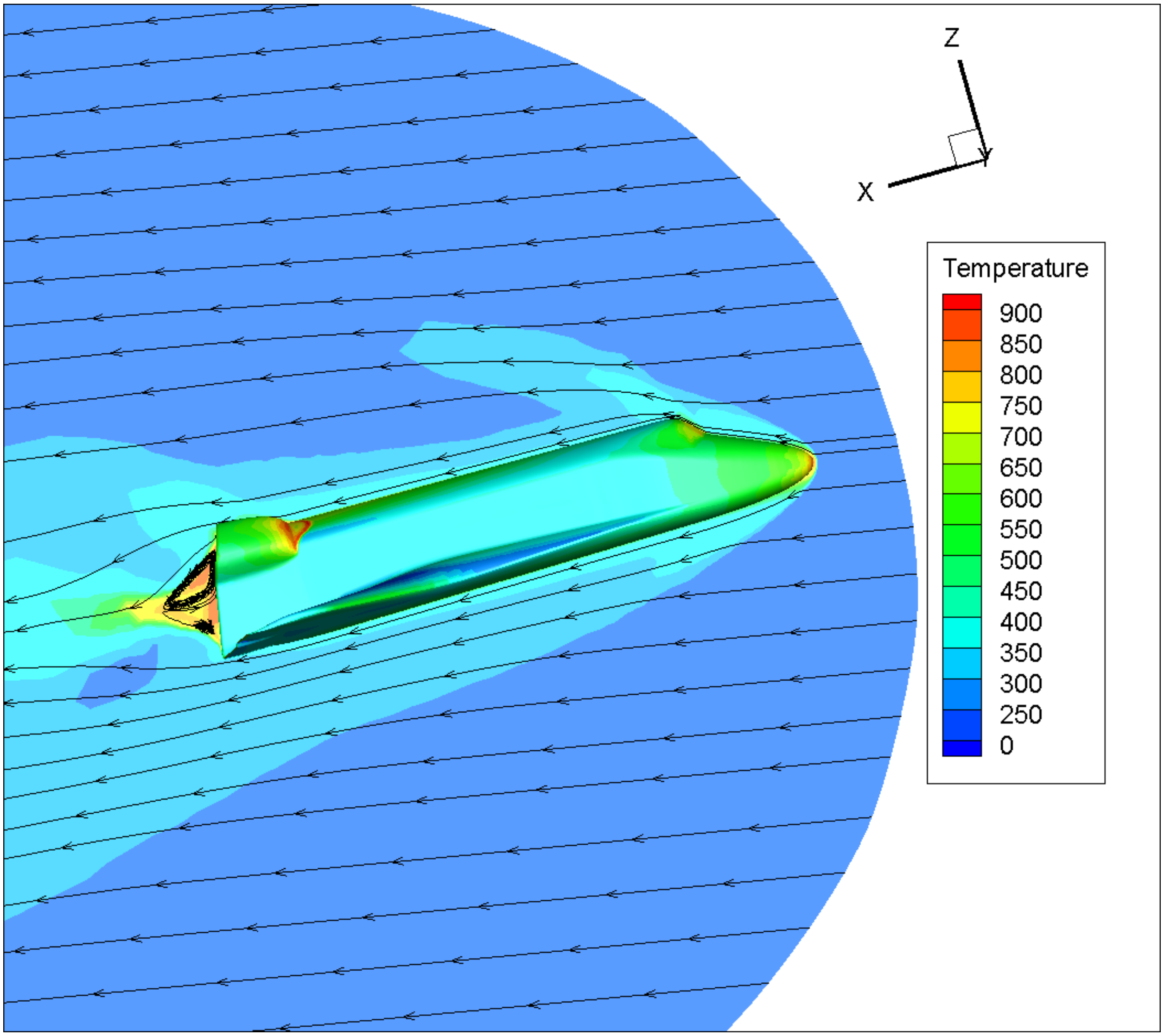

Figure 10: Temperature contour at the symmetry plane of the orbiter at 10 degs AoA

3.4.2 AoA = 20°

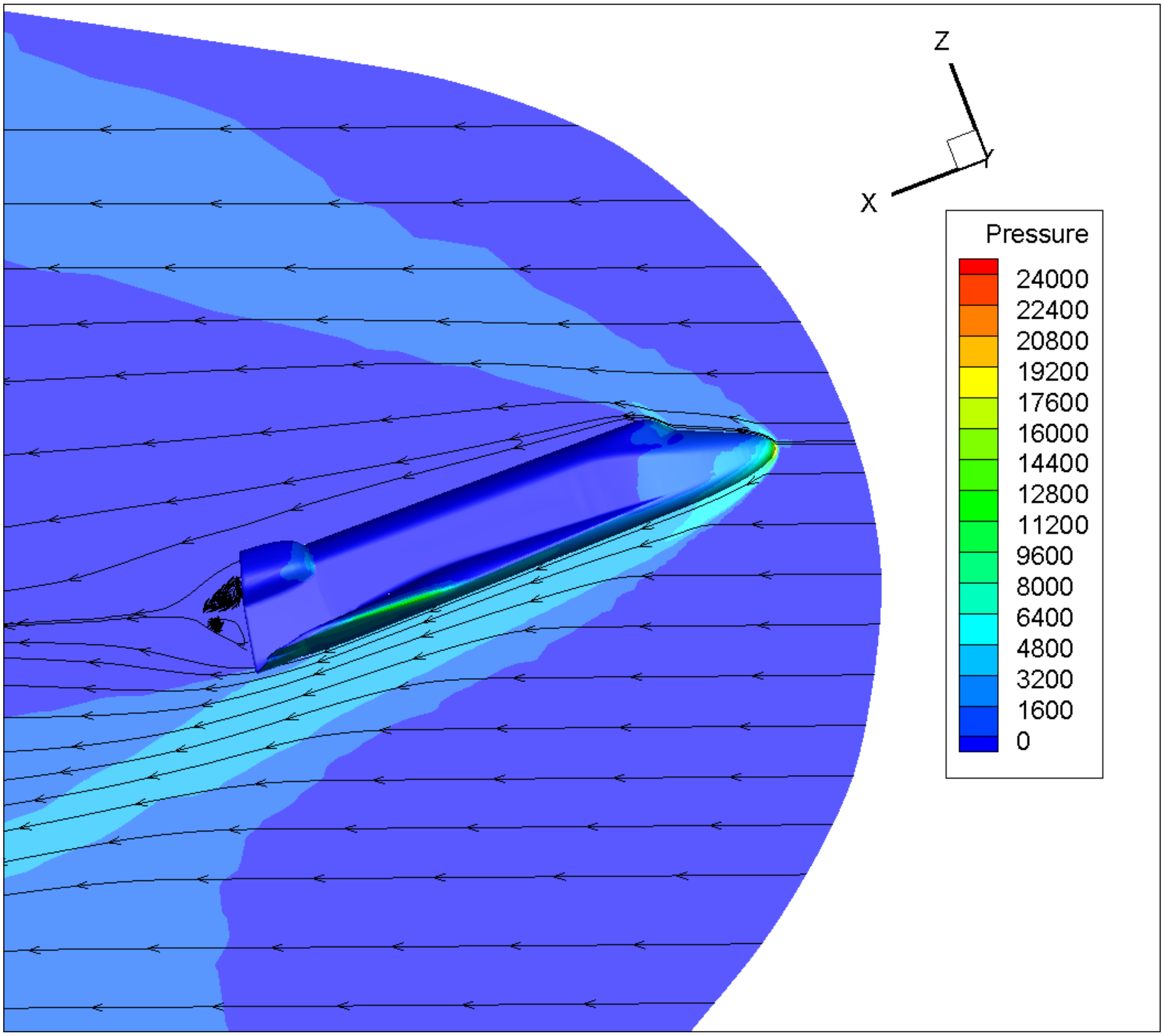

Figure 11: Pressure contour at the symmetry plane of the orbiter at 20 degs AoA

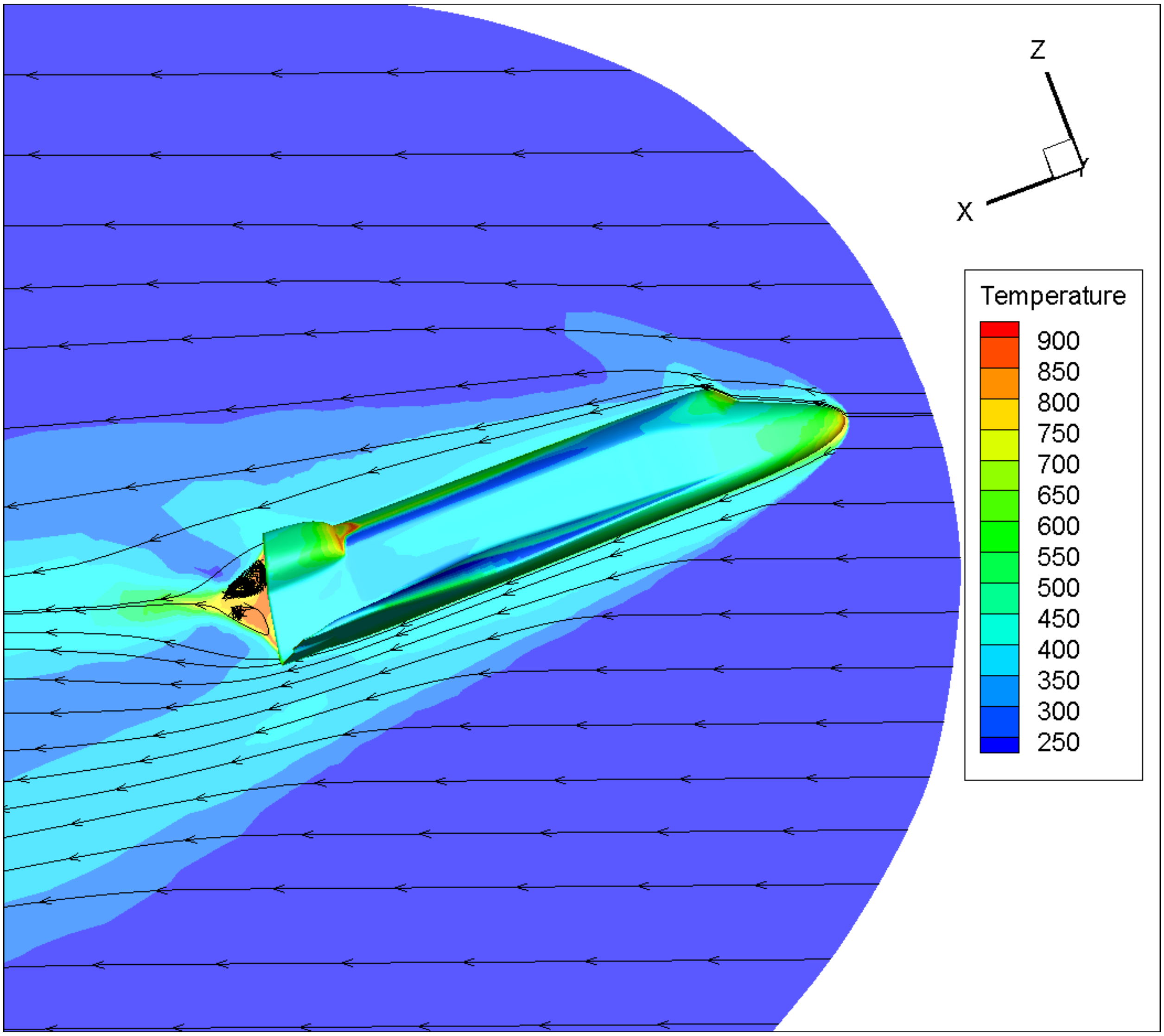

Figure 12: Temperature contour at the symmetry plane of the orbiter at 20 degs AoA

3.5 Results of grid adaptation

3.5.1 Side by side of contour plots

3.5.2 Side by side of mesh

3.5.3 Table of force coefficients

3.5.4 Fluent settings used to adapt grid

Appendix

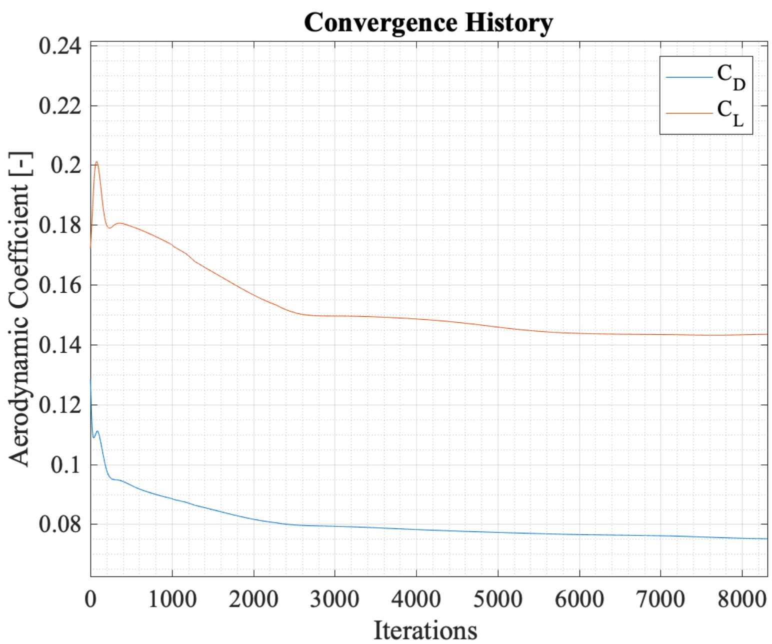

Figure 13: Convergence history for AoA = 10°

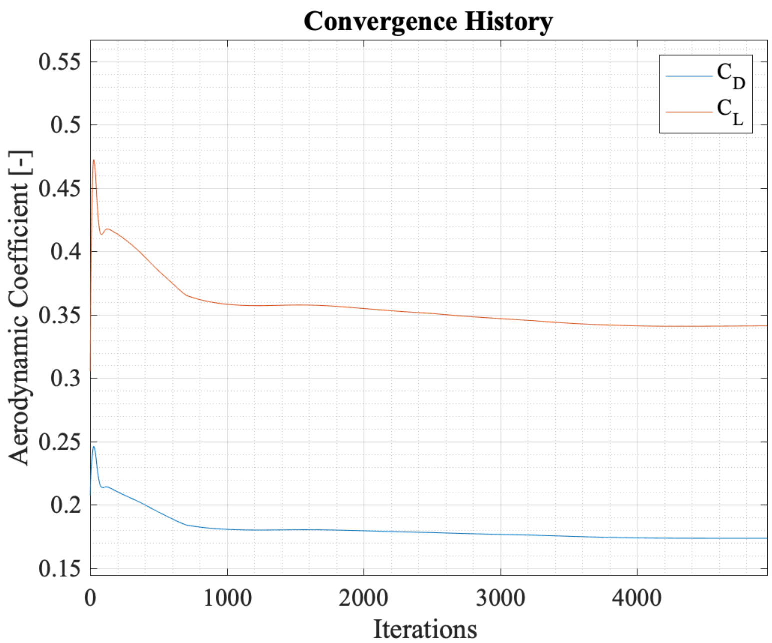

Figure 14: Convergence history for AoA = 20°

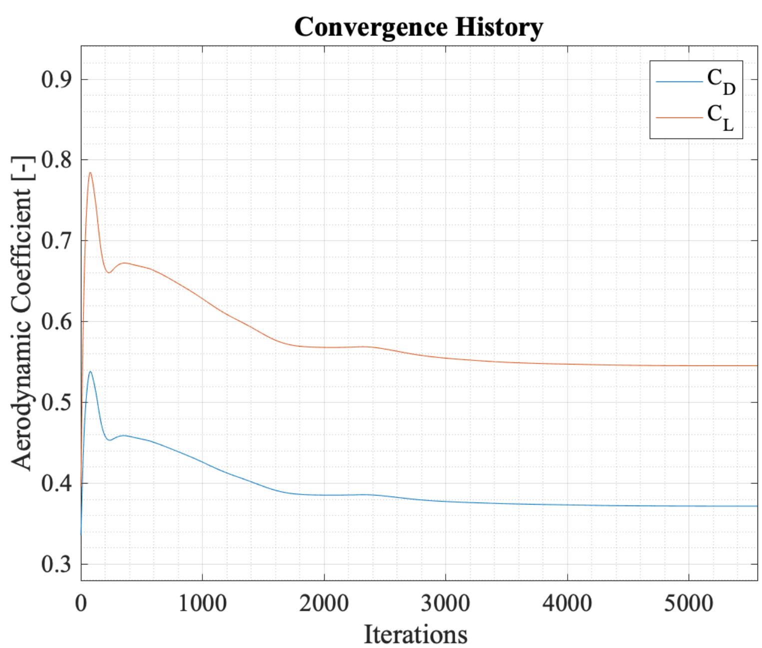

Figure 15: Convergence history for AoA = 30°

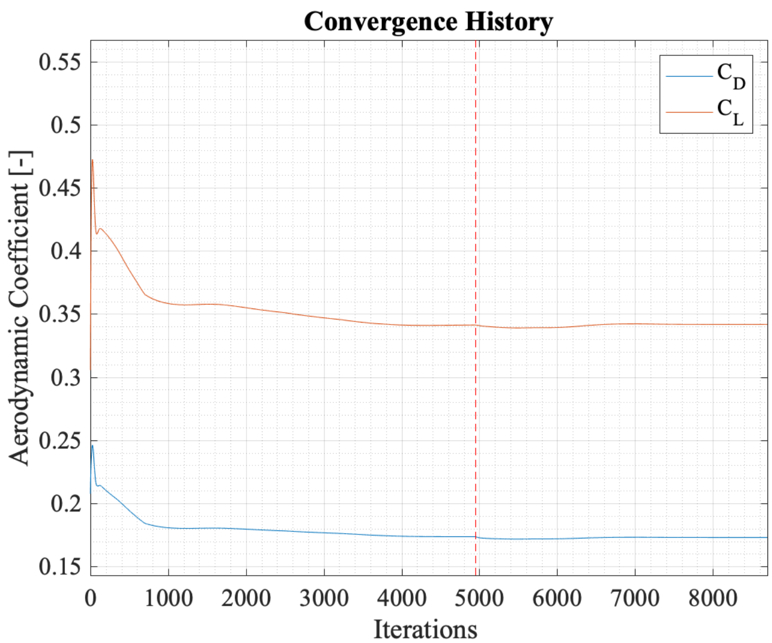

Figure 16: Convergence history with adaption for AoA = 20°; red dashed-line indicates where iterations for the refined mesh began.

References

[1] John D. Anderson. *Modern Compressible Flow with Historical Perspective.* McGraw Hill Education, 2003.

[2] Rui Dilão and João Fonseca. Dynamic guidance of gliders in planetary atmospheres. *American Society of Civil Engineers*, 1(29), 1 2016.